Study of Condensed Matter by Neutron Scattering and Complementary Methods

AC Susceptibility Studies of Phase Transitions and Magnetic Relaxation: Conventional, Molecular and Low-Dimensional Magnets

M. Bałanda*
Institute of Nuclear Physics, Polish Academy of Sciences, Kraków, Poland

Dedicated to the memory of Professor Jerzy Janik

The paper presents the review of AC susceptibility measurements in study of magnetic phase transitions and spin dynamics. Examples of several types of phase transitions in conventional and molecular magnets are shown. The phenomenon of magnetic relaxation is briefly ascribed and illustrated with results on relaxation in low-dimensional molecular magnets, such as single molecule magnets, single chain magnets and quasi 1-dimensional systems showing magnetic phase transition to the long-range ordered phase. The following experimental possibilities of the AC technique, which allow to get insight into properties of novel magnetic materials are mentioned: (i) change of the AC field amplitude (in order to distinguish ferro-(ferri) and antiferromagnets); (ii) use of a static field $H_{\rm DC}$ (to conclude on the type of magnetic order and to study the phase diagram); (iii) measurement of nonlinear susceptibilities (to conclude on the type of phase transition); (iv) probing the dependence of both components of susceptibility on frequency of the AC field (to study magnetic relaxation); (v) tests of the DC field effect on the frequency dependence of $\chi_{\rm AC}$ (to analyze the possibility of blocking or reentrant spin-glass transition).

DOI: 10.12693/APhysPolA.124.964
PACS: 75.30.Cr, 75.30.Kz, 75.40.Gb, 75.50.−y

1. Introduction

During last two decades of research on magnetism of condensed matter, many novel materials were obtained and new types of behaviour and magnetic order have been found. Besides basic classes of magnetism i.e. diamagnetism, paramagnetism, ferromagnetism, antiferromagnetism and ferrimagnetism, and those recognized later, like metamagnetism, helimagnetism, spin glass, or superparamagnetism, nowadays one deals with various kinds of nanostructured or molecule-based magnetic materials. There are nanoparticles and ferrofluids, nanowires, thin films or multilayers, molecular magnets and nanomagnets, all of them showing new interesting properties.

A sensitive and relatively less used tool for characterizing new materials is the dynamic magnetic susceptibility technique, also called AC susceptibility, $\chi_{\rm AC}$. $\chi_{\rm AC}$ is complementary to the measurements in the static (DC) magnetic field and becomes indispensable especially for investigations of phase transitions and magnetic relaxation. AC susceptibility is the differential $\mathrm{d}M/\mathrm{d}H$ response of the magnetization (M) of the sample to an oscillating magnetic field (H). Operating frequencies f vary most often from 1 Hz (to compare with static susceptibility) up to 10 kHz. The low amplitude of the driving field is used to probe the undisturbed ground state of the investigated system. Apart from oscillating magnetic field, the DC bias field may be applied. Since the invention [1], the method was frequently used for studies of paramagnetic salts [2], weak and low dimensional magnets [3], spin glasses [4] and $\mathrm{HT_c}$ superconductors [5]. Besides investigation of the relaxation effects, measurements of AC magnetic susceptibility are used for studying phase transitions to the ordered state, spin reorientation or metamagnetic transitions. The method is also used to analyse change in anisotropy energy.

AC susceptibility is a complex value and reads

$$\chi_{\rm AC} = \chi' - \mathrm{i}\chi'', \tag{1}$$

where the real component χ', related to the reversible magnetization process, stays in-phase with the oscillating field

$$H(t) = H_0 + h\cos(2\pi f t). \tag{2}$$

The imaginary component χ'' is related to losses due to the irreversible magnetization process and energy absorbed from the field, as the phase shift θ may occur in magnetization $M(t)$ in respect of $H(t)$ given

$$M(t) = M_0 + m\cos(2\pi f t - \theta). \tag{3}$$

In this way

$$\chi' = m\cos\theta/h, \tag{4}$$

$$\chi'' = m\sin\theta/h. \tag{5}$$

Components χ' and χ'' of the susceptibility of a magnetic sample are functions of temperature and may depend on the frequency f and amplitude h of the driving field, static bias field H_0, applied pressure and other external parameters. Irreversibility is a result of relaxation processes of various origin, like the irreversible movement of domain walls, small hysteresis loop in ferromagnets, spin lattice relaxation in paramagnets, relaxation of superparamagnets or flux creep in superconductors. Relaxation time, or its distribution, may be determined

*e-mail: Maria.Balanda@ifj.edu.pl

from the relation between real and imaginary components of χ_{AC} (Argand plot). Dependence $\chi'(2\pi f)$ is called *magnetic dispersion*, $\chi''(2\pi f)$ is called *magnetic absorption*. Additional information on phase transition may be obtained from nonlinear susceptibilities, as in general case

$$M(H) = M_0 + \chi_1 H + \chi_2 H^2 + \chi_3 H^3 + \ldots, \qquad (6)$$

where χ_1 — linear (first order), χ_2 — second order, χ_3 — third order susceptibilities. Nonlinear χ_2 and χ_3, determined from the signals detected at the frequency $2f$ and $3f$, are called second (2hr) and third (3hr) harmonics and are expressed as $\frac{1}{2}\chi_2 h$ and $\frac{3}{4}\chi_3 h^2$, respectively. Nonlinear contribution to magnetization becomes usually larger at temperatures close to the temperature of the long range magnetic ordering T_c. Peak in the third harmonic confirms the occurrence of the magnetic phase transition (e.g. paramagnetic to ferromagnetic, or paramagnetic to spin-glass state), while the second harmonic is observed only for samples with a spontaneous magnetization.

The paper presents the review on the representative AC susceptibility results obtained using the commercial LakeShore 7225 Susceptometer. The following experimental possibilities were used to get deeper insight into phase transitions and/or dynamics of the spin systems under study: (i) change of the AC field amplitude (in order to distinguish ferro-(ferri) and antiferromagnets); (ii) use of a static field H_{DC} (to conclude on the type of magnetic order and to study the phase diagram); (iii) measurement of nonlinear susceptibilities (to conclude on the type of phase transition); (iv) probing the dependence of both components of susceptibility on frequency of the AC field (to study magnetic relaxation); (v) tests of the DC field effect on the frequency dependence of χ_{AC} (to analyze the possibility of blocking or reentrant spin-glass transition). Examples of several types of magnetic phase transitions in conventional and molecular magnets are shown. The phenomenon of magnetic relaxation is briefly ascribed and illustrated with results on relaxation in molecular and low-dimensional magnets. A special attention is paid to slow relaxation in single molecule magnets (SMM), single chain magnets (SCM) and also in quasi 1-dimensional systems showing magnetic phase transition to the long-range ordered phase.

2. Examples of magnetic phase transitions as recorded by AC susceptibility

2.1. Ferromagnetic to paramagnetic phase transition

Figure 1 presents the temperature dependence of the AC magnetic susceptibility (measured with h = 3 Oe, f = 80 Hz) at the transition from a ferromagnetic to the paramagnetic state for the molecule-based $\{[Fe^{II}(H_2O)_2]_2[Nb^{IV}(CN)_8]\cdot 4H_2O\}$ magnet [6]. The DC susceptibility measured at H_{DC} = 2 kOe is shown for comparison. The related temperature derivatives are depicted in the inset. The substance is an example of the isotropic three-dimensional (3D) ferromagnet. As shown, the measurement of χ_{AC} assures precise determination of the temperature of the long range magnetic ordering T_c. T_c may be determined from the $d\chi'/dT$ minimum, the χ'' onset or from the χ' maximum. Usually the temperatures of $d\chi'/dT$ minimum and of χ'' onset coincide, which is the case also here.

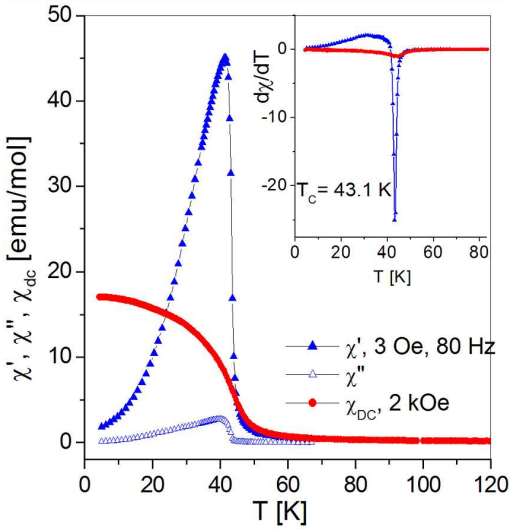

Fig. 1. AC and DC magnetic susceptibility at the transition from a ferromagnetic to the paramagnetic state for the molecular $[Fe^{II}(H_2O)_2]_2[Nb^{IV}(CN)_8]\cdot 4H_2O$ 3D ferromagnet [6]. The related temperature derivatives $d\chi'/dT$ and $d\chi_{DC}/dT$ are depicted in the inset.

2.2. Unique phase transition in quasi two-dimensional system with XY anisotropy

Thanks to the modern synthetic chemistry molecular magnets of different dimensionality may be obtained: three-dimensional (3D) magnets, two-dimensional (2D) layered systems, one-dimensional molecular chains (1D) or high-spin molecules (0D). The two-dimensional molecular networks are attractive due to their distinctive phase diagram in the applied field and as an alternative source of technologically important magnetic multilayers.

Interesting behaviour was found by us [7, 8] for the quasi-2D copper octacyano-tungsten compound $(tetrenH_5)_{0.8}Cu_4[W(CN)_8]_4\cdot xH_2O$, where both Cu- and W-ions carry spin $s = 1/2$. The bilayered structure of the compound consists of anionic $Cu_4[W(CN)_8]_4$ double-layers aligned in the ac plane with tetren countercations and water molecules located between the sheets. Unit cell is orthorhombic with approximate dimensions of $a = 7.4$ Å, $c = 7$ Å, $b = 32$ Å, and the distance between the double-layers of ≈ 10 Å.

As follows from the Mermin–Wagner theorem [9], the 2D isotropic Heisenberg magnet can have the transition to the ordered state only at $T_c = 0$ K, while for the 2D system with XY anisotropy, the topological Kosterlitz and Thouless transition [10], caused by the unbinding of vortex-antivortex pairs, may take place at a critical temperature T_{KT}.

Magnetic susceptibility χ_{AC} of the $(tetrenH_5)_{0.8}Cu_4[W(CN)_8]_4{\cdot}xH_2O$ powder sample and χ_{DC} of the single crystal (parallel and perpendicular to the layers) measured in field of 2 kOe are depicted in Fig. 2. As is seen, this quasi-2D spin system undergoes the phase transition at $T = 33.3$ K. The DC susceptibility measured in the ac plane is almost one order of magnitude larger than that perpendicular to the bilayers. The exceptionally narrow χ_{AC} peak measured for the powder sample with $h = 2$ Oe and $f = 125$ Hz, is still three times stronger. The χ_{AC} drops suddenly just below T_c and levels off at a low value, it also does not depend on frequency as checked in the range of 5–10 000 Hz. The thorough analysis of magnetization in paramagnetic and in the ordered phase brought evidence of the Kosterlitz–Thouless type of the transition [7]. Thanks to the small amplitude of the AC field, from χ_{AC} we could precisely determine the γ critical exponent ($\chi \propto \varepsilon^{-\gamma}$, where $\varepsilon = |T/T_c - 1|$, $T > T_c$) and get complementary proof of the type of our spin system. The value $\gamma = 1.31 \pm 0.1$ obtained from the $\chi'(\varepsilon)$ log–log fit (see inset to Fig. 4) is almost equal to that predicted for a spin system with XY anisotropy.

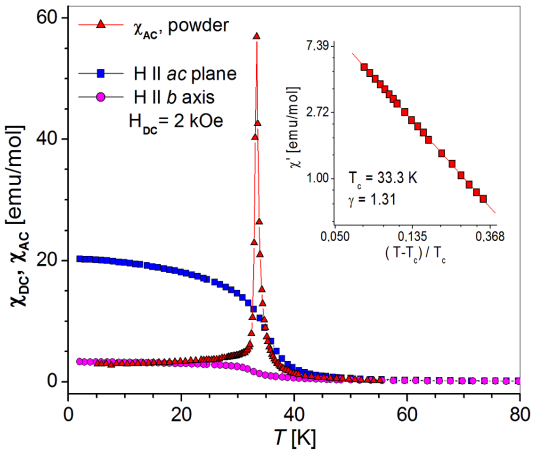

Fig. 2. Single crystal DC and powder AC susceptibility of the bilayered quasi-2D $(tetrenH_5)_{0.8}Cu_4[W(CN)_8]_4{\cdot}xH_2O$ molecular magnet; inset: the χ_{AC} critical scaling plot [7].

2.3. *Commensurate to incommensurate order transition*

In the intermetallic compound $TbCo_2Si_2$ cobalt is nonmagnetic and only Tb-moments are ordered with $T_N = 46$ K [11]. Temperature dependences of χ' and $d\chi'/dT$ for this compound are displayed in Fig. 3. As expected for the antiferromagnetic structure, imaginary component χ'' is almost zero. The temperature T_N is marked on the $d\chi'/dT$ curve as the centre of a well-defined fall-down and is equal to 45 K. An anomaly in the $d\chi'/dT$ curve may not arise from the spin reorientation since such transitions are usually clearly seen in the χ' vs. T dependences, which is not the case here. Thus, the observed anomaly comes probably from the transformation from the antiferromagnetic collinear to the sine-wave modulated incommensurate structure. The anomalous behaviour of $d\chi'/dT$ starts at $T_t = 42$ K. This transition has been also observed by neutron diffraction and heat capacity measurements.

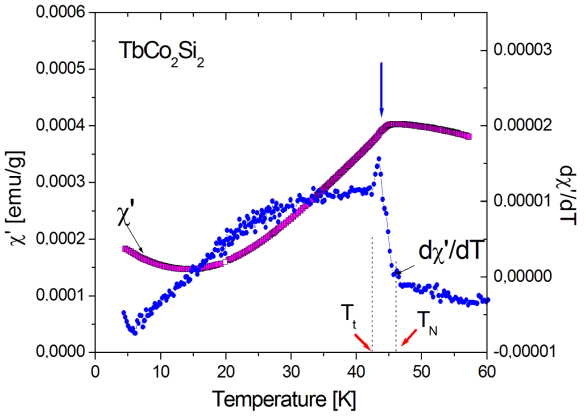

Fig. 3. Temperature dependence of χ' and of $d\chi'/dT$ for $TbCo_2Si_2$ [11].

2.4. *Spin glass transition above T_N identified with higher harmonics of χ_{AC}*

As described in [12], magnetic susceptibility of a frustrated antiferromagnet TbAuIn shows two anomalies, the first of which, occurring at 33 K, is a Néel point, confirmed with neutron diffraction studies. The other anomaly, present at 48 K, i.e. above T_N, was a rare effect, difficult to explain (see Fig. 4). The only method which revealed also some anomalous behaviour in TbAuIn in this temperature range was the resistivity measurement.

In order to get a deeper insight into phase transitions of Tb uIn, the second and third harmonics were measured for the fundamental frequency $f = 120$ Hz. The magnitude of harmonics was less than 0.01% of the linear one (Fig. 5). The 2hr and 3hr exhibited a double peak at about 50 K, whereas the F transition was visible only in 3hr. These data allowed to inscribe the strange transition to the spin-glass one with $T_g = 52$ K. Because 2hr was present, one could conclude that the glass phase coexisted with the ferromagnetic phase. Transition at 52 K is therefore of magnetic disorder–disorder origin. Strong influence of the external magnetic field and driving field frequency on the position, as well as on the magnitude of the AC susceptibility anomaly (not shown here) confirmed it to be the cluster-glass to paramagnetic phase transition. Diffuse neutron scattering observed for TbAuIn at temperatures above the T_N supports the conclusion of the existence of cluster-glass state [13].

2.5. *χ_{AC} dependence on AC field amplitude and frequency in rare earth metals and intermetallics*

AC susceptibility is also very helpful in investigations of rare earth (RE) metals and of intermetallic compounds

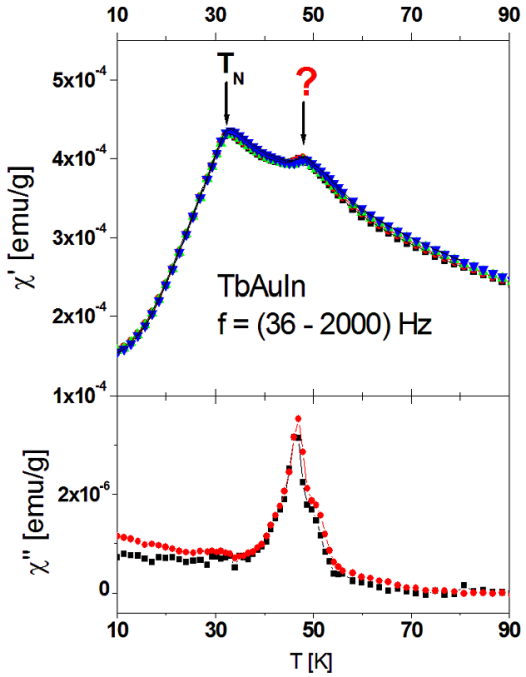

Fig. 4. Temperature dependence of real and imaginary χ_{AC} components for TbAuIn [12].

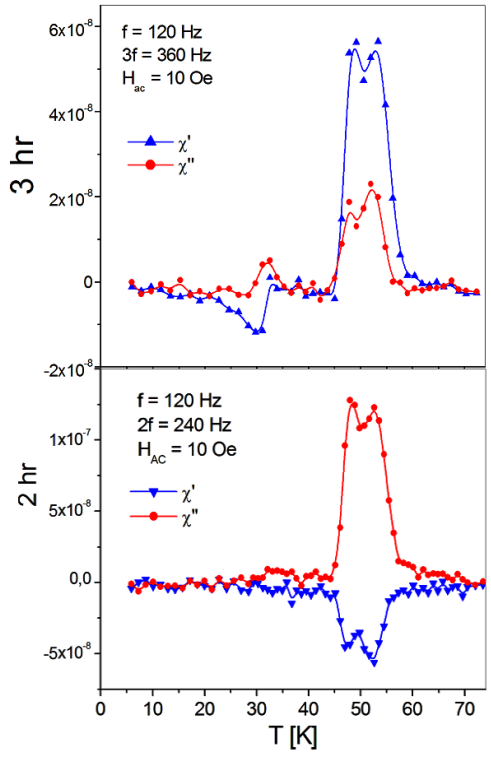

Fig. 5. Nonlinear susceptibilities for Tb uIn: transition at T_N is detected only with 3hr, while cluster glass phase with $T_g \approx 52$ K is marked with anomalies of both harmonics [12].

of rare earth metals with $3d$, $4d$, or $5d$ elements. Below we present results obtained for two intermetallic systems and for two pure $4f$ metals, Gd and Th.

Intermetallic compounds of rare earth metals with $3d$, $4d$, or $5d$ elements are usually complex ferrimagnets, in which competing ferro- and antiferromagnetic interactions lead to transitions between the phases with different magnetic structures. χ_{AC} measurements, carried out with different h, provide information on the temperatures and type of the transitions.

Figure 6 shows the result for the ferromagnetic GdPdIn with $T_{AC} = 102$ K crystallizing in the hexagonal ZrNi l-type structure [14]. Like for Gd, both χ_{AC} components increase with h. The anomaly at the temperature close to T_{AC} reflects the Hopkinson effect, frequently observed for ferrites. The anomaly may arise in the case of strong decrease of anisotropy constant K with temperature, because, generally $\chi_{AC} \propto M_s^2/K$ (see Sect. 3.3). One should also note the large χ'', which is equal to about 10% of χ'.

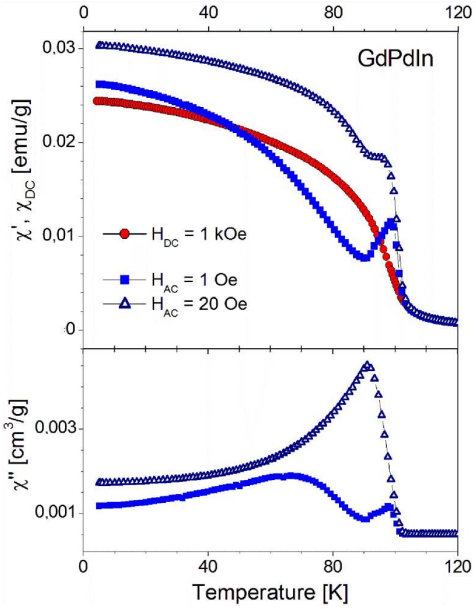

Fig. 6. Temperature dependence of χ' and χ'' measured with $H = 1$ Oe and 20 Oe for ferromagnetic GdPdIn; the DC susceptibility (in $H_{DC} = 1$ kOe) is shown for comparison [14].

Susceptibility measured for the related compound DyPdIn is depicted in Fig. 7. It shows two maxima: at $T_c = 34$ K and the second at $T_t = 14$ K, which behave differently when AC field amplitude is changed. The χ' anomaly at T_c is accompanied by large χ'' (*ca.* 10% χ') and both components depend strongly on h. Such behaviour indicates that on cooling from the paramagnetic phase, long range ferrimagnetic ordering appears at T_c. It is also seen that with rising h from 1 Oe up to 20 Oe, position of the χ' peak shifts towards lower temperatures, while χ'' peak shifts down even more than 2 K.

The anomaly at $T_t = 14$ K reflects transition to the antiferromagnetic or slightly uncompensated FM-phase (negligible χ''). Thus, in ferro- or ferrimagnetic phase the imaginary component is present, while in the antiferromagnetic phase χ'' is zero.

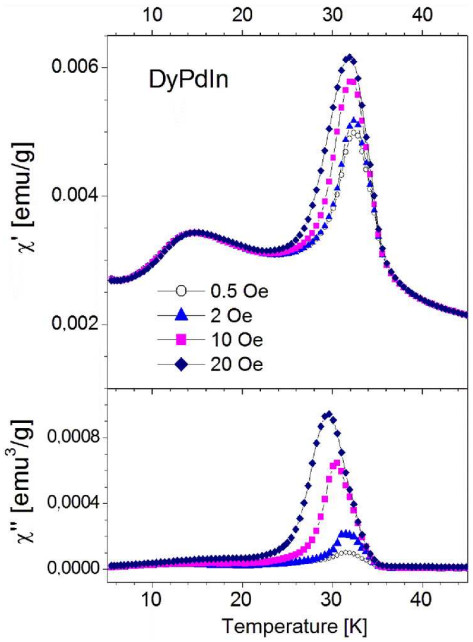

Fig. 7. Temperature dependence of χ' and χ'' for DyPdIn ferrimagnet measured with varied H (shown); at $T_t = 14$ K the FI-FM transition occurs [14].

Gadolinium is a ferromagnet with $T_{AC} = 293.4$ K. At $T = 225$ K, the anisotropy constant changes sign and spin reorientation takes place with magnetic moments parallel to the c-axis for $T > T_{SR}$ and perpendicular to the c-axis for T below T_{SR} [15]. Figure 8 shows χ' and χ'' measured with two amplitudes of the driving field [16]. Both χ' and χ'' components increase with h. The spin reorientation point is clearly seen as the temperature at which the χ' curves merge as χ' at T_{SR} does not depend on h. At $T = T_{SR}$ the χ'' component has minimum. The χ_{AC} results reported for Gd single crystal [17] detect T_{SR} as a weak χ' maximum and a kink when measured with the AC field parallel to the c-axis and as a maximum of χ' for AC field perpendicular to c-axis. Thus, it appears that T_{SR} may be determined with a good accuracy also for the polycrystalline bulk sample with the h-dependent measurement.

Figure 9 shows the χ_{AC} data measured with varied frequency, obtained for the polycrystalline sample of thulium [16]. Thulium orders at $T_N = 58$ K with a sinusoidal modulation of the c-axis component of the magnetic moments [15].

As shown in Fig. 7, T_N does not depend on frequency and χ'' component is absent, as it should be for the antiferromagnet. Below 38 K, magnetic moment modulation begins to square off and a system transforms to the complex ferrimagnetic structure, with four moments up along c-axis followed by three moments down [15].

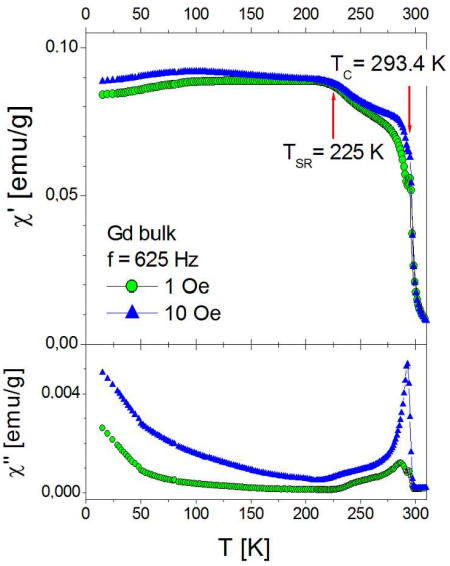

Fig. 8. χ' and χ'' of polycrystalline bulk Gd measured at $f = 625$ Hz with two amplitudes of AC field. Spin reorientation and Curie temperatures are indicated.

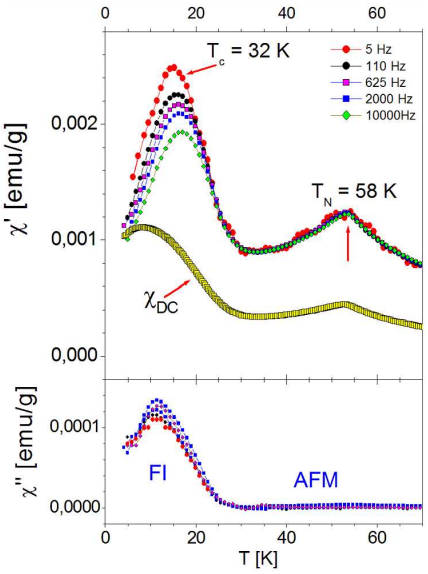

Fig. 9. χ' and χ'' of polycrystalline Tm measured with varied frequency. Ferrimagnetic and Néel temperatures are indicated. DC susceptibility in the field 2 kOe is shown for comparison.

Figure 9 indicates that at transition to the ferrimagnetic phase the χ'' component appears, and both χ' and χ'' are frequency dependent. Therefore it appears that transition to the ferrimagnetic phase is not the immediate process and that the relevant reorganization of the domain structure is a relaxation effect with the time scale of $\approx 10^{-5} \div 1$ s. Magnetic relaxation will be discussed

in the next paragraph. We would like to add that very weak χ_{AC} dependence on h was observed only in the ferrimagnetic phase.

3. Relaxation in magnetic systems

3.1. Brief description

After a change in the applied magnetic field from H to $H \pm \Delta H$, magnetization M of a spin system will reach a new equilibrium state after characteristic time τ, called the relaxation time. Relaxation process consists in energy exchange between the spins and other degrees of freedom, which proceeds through the movement of domain walls, rotation of magnetic moments, nucleation of regions with reverse magnetization and other effects. In the simplest case, magnetic relaxation is defined by means of one energy barrier and one relaxation time, where the time dependence of magnetization is the exponential function $M(t) = M_0 \exp(-t/\tau)$ (for magnetization decay). Usually, relaxation is a complex phenomenon with the large time scale involved. Study of relaxation provides insight into magnetic structure and spin–lattice interactions in the sample.

The thermodynamic model for relaxation of a magnetic system in the oscillating magnetic field parallel to a constant field H_0 was derived by Casimir and du Pré [18]. According to the model, in thermal equilibrium, the temperature T_{s} of the spin system and that of the lattice, T_{l}, are equal. As a result of a field change, T_{s} will change from its equilibrium value. Subsequently, spin–lattice relaxation will take place and heat will be exchanged between the spins and the lattice. From the entropy change of the process, in which magnetic field changes periodically with frequency $f = \omega/2\pi$, one obtains expression for the complex susceptibility

$$\chi(\omega) = \chi_{\mathrm{S}} + \frac{\chi_{\mathrm{T}} - \chi_{\mathrm{S}}}{1 + \mathrm{i}\omega\tau}, \tag{7}$$

where χ_{T} is an isothermal susceptibility in the limit of the lowest frequencies and is related to spin–lattice relaxation; χ_{S} is related to spin–spin relaxation and is an adiabatic susceptibility in the limit of the highest frequencies, for which the magnetic system remains isolated from surrounding. Exchange of energy between spins is several orders quicker than that between the spins and the lattice. For a paramagnet in zero field $\chi_{\mathrm{T}} = \chi_{\mathrm{S}}$.

Complex $\chi(\omega)$ has real and imaginary components

$$\chi'(\omega) = \chi_{\mathrm{S}} + \frac{\chi_{\mathrm{T}} - \chi_{\mathrm{S}}}{1 + \omega^2\tau^2}, \tag{8}$$

$$\chi''(\omega) = (\chi_{\mathrm{T}} - \chi_{\mathrm{S}})\frac{\omega\tau}{1 + \omega^2\tau^2}. \tag{9}$$

The frequency dependence of χ' and a non-zero χ'' signal are always a consequence of one or more relaxation processes with characteristic relaxation time constants. The highest χ'' (up to 50% of χ') is reached when a relaxation process with one time constant takes place. Low values of χ'' in spin-glasses suggest a distribution of relaxation time constants.

The relaxation time τ or the distribution α of relaxation times may be determined from the χ'' vs. χ' plot for a given temperature and different ω; this is the so-called Argand plot (or Cole–Cole plot). In the case of one relaxation time (the Debye process) the plot is a semicircle, while for the distribution of relaxation times the χ'' vs. χ' plot is an arc. The central angle of the arc is equal to $(1-\alpha)\pi$, where α is a measure of the distribution of the relaxation times. For the Debye process $\alpha = 0$, while for spin glasses it can reach the value 0.9. The Cole–Cole expression modified for the distribution of relaxation times reads

$$\chi(\omega) = \chi_{\mathrm{S}} + \frac{\chi_{\mathrm{T}} - \chi_{\mathrm{S}}}{1 + (\mathrm{i}\omega\tau)^{1-\alpha}}. \tag{10}$$

The angular frequency ω, at which the absorption reaches its maximum $\chi''(\omega) = \frac{1}{2}(\chi_{\mathrm{T}} - \chi_{\mathrm{S}})$, determines the relaxation time τ of the relevant relaxation process as $\tau = \omega^{-1}$. The Cole–Cole approach concerns a distribution of relaxation times that is symmetric on the logarithmic time scale. From that analysis performed at different temperatures one obtains the temperature dependence of the relaxation time $\tau(T)$.

Magnetic moments are coupled to the crystal lattice through the spin–orbit interaction. Exchange of energy between magnetic moments and a lattice occurs via phonons and magnons. All processes, in which phonons or magnons take part, depend on temperature, this is why the spin–lattice relaxation time decreases with temperature. Depending on the magnetic system, temperature dependence of the relaxation time may be described by different functions (laws):

- the Arrhenius law

  $$\tau(T) = \tau_0 \exp\left(\Delta E/k_{\mathrm{B}}T\right), \tag{11}$$

  for thermally activated processes, which are typical for superparamagnets; ΔE is the energy barrier for (macro)spin reversal, τ_0 is the characteristic time, related to the natural frequency of gyromagnetic precession; time τ_0 is considered as temperature independent and equals from $\approx 10^{-9}$ s for nonmetallic to 10^{-13} s for metallic systems;

- the Vogel–Fulcher law

  $$\tau(T) = \tau_0 \exp\left(\Delta E/k_{\mathrm{B}}(T - T_0)\right) \tag{12}$$

  is typical for (cluster)spin-glasses or ferrofluids and includes inter-cluster or inter-particle interaction;

- the generalized Vogel–Fulcher law

  $$\tau(T) = \tau_0 \exp\left(\Delta E/k_{\mathrm{B}}(T - T_0)^z\right) \tag{13}$$

  introduces the critical exponent and becomes relevant at temperatures close to phase transition;

- the critical scaling formula

  $$\tau(T) \propto (T - T_0)^{zv} \tag{14}$$

  describes approach to the spin-glass freezing.

Value of the barrier ΔE and its dependence on the properties of the material, like domain structure, domain pinning or anisotropies, is crucial for the dynamics of the spin system. Attempt time τ_0 may depend slightly on the applied field and may differ for the specific group of substances.

3.2. Relaxation in paramagnets

At high temperatures, in zero DC field and low frequencies of AC field, the paramagnetic spin system follows the oscillating field and no relaxation is observed. When $H_{\mathrm{DC}} \neq 0$ the spin–lattice relaxation appears, related mainly to the direct process of the emission or absorption of one phonon. When the frequency of the oscillating magnetic field increases, additional absorption appears which is connected with the relaxation within the spin system. The spin–spin relaxation time, τ_{S}, is much lower than spin–lattice relaxation time $\tau_{\mathrm{S-L}}$ and does not depend on temperature. The basic mechanism for spin–spin relaxation is of a magnetic dipolar type. The approximate relaxation time for this type of coupling is $\tau_{\mathrm{S}} \approx 10^{-10}$ s; it is understood as the time necessary for changing the direction of the precession axis.

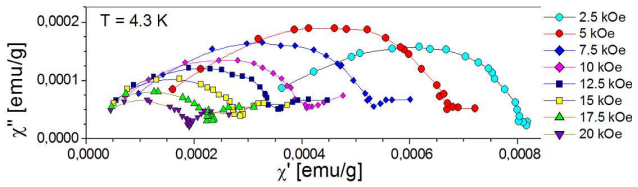

Fig. 10. Argand plots for $CrK(SO_4)_2{\cdot}12H_2O$ at $T = 4.3$ K showing magnetic relaxation at different DC bias fields (shown) and AC frequencies ranging from 5 Hz up to 10 kHz.

Figure 10 shows relaxation in the AC field of the paramagnetic $CrK(SO_4)_2{\cdot}12H_2O$ (alum) when bias DC field is applied. The Argand diagrams were obtained for f between 5 Hz (highest χ', first points on the right) and 10000 Hz (smallest χ', last points on the left), for several values of the constant external field at $T = 4.3$ K. The plots are flattened, showing that more than one relaxation process occur. One expects here three processes: the slowest process emerges starting from $H = 5$ kOe, the second process occurs with the average time constant and is the strongest one, the third process is expected (on the left-hand side of the curves) and is not accessible with our setup. The relaxation time for the average relaxation process, given by the frequency of the highest χ'' value, does not change much as the field is increased: for $H = 2.5$ kOe $\tau \approx 10^{-3}$ s, while for $H = 20$ kOe $\tau \approx 5 \times 10^{-4}$ s. The main effect is the decrease of the isothermal susceptibility; however, in order to determine $\chi_{\mathrm{T}}(H)$ precisely, frequencies lower than 5 Hz should be used. The expected third process would probably be due to some type of spin–spin relaxation for crystal-field-resolved $s = 3/2$ Cr^{3+} multiplet [19].

3.3. Relaxation in long-range ordered magnets

In order to observe the spin–lattice relaxation in paramagnets, the non-zero applied magnetic field is needed, whereas in magnetically ordered materials the internal magnetic fields are present due to the exchange coupling of the spins. AC susceptibility of the long-range ordered magnets comes from the spins in the domains and spins in the domain walls. Contribution from domain walls is more significant because spins in the wall, which are in their subtle equilibrium state, should respond easily to the AC field even at high frequencies. As discussed in [19, 20], susceptibility resulting from the small amplitude motion of domain walls can be derived from the equation of motion, similar to that of a damped harmonic oscillator. The domain wall susceptibility, which is the difference between the isothermal and adiabatic susceptibility, $\chi_{\mathrm{w}} = \chi_{\mathrm{T}} - \chi_{\mathrm{S}}$ is equal to

$$\chi_{\mathrm{w}} = \frac{4M_{\mathrm{s}}^2 d_{\mathrm{w}}}{KL}, \tag{15}$$

where M_{s} is the magnetization of saturation, d_{w} is the domain wall width, K is an anisotropy constant, and L is the distance between two domains.

Temperature dependence of χ_{w} is contained in two parameters, M_{s} and K, as the distance L between two domains stays almost constant up to temperatures very close to T_{c}. Anisotropy K is expected to decrease with temperature, while $M_{\mathrm{s}}(T)$, given by the Brillouin function, is constant at low temperatures and goes to zero at T_{c}. In that way, one usually observes the increase of χ_{w} with temperature, but the behaviour close to T_{c} may be more complex, like the Hopkinson effect mentioned in Sect. 2.5.

The effects, which contribute to losses and therefore to relaxation may be the following: irreversible wall displacements, irreversible magnetization rotation (hysteresis loss), eddy currents, diffusion of electrons or deffects. The big χ'' losses connected with the domain structure reconstruction were reported for $4f{-}3d$ hard magnets [21]. One should note that for strong ferro- or ferrimagnets with T_{c} up to 1000 K, e.g. ferrites, frequency dependence of AC susceptibility is observed for large frequencies $f \approx 10^5{-}10^6$ Hz.

3.4. Relaxation in spin-glasses

AC susceptibility is an important technique for investigating spin-glasses as no information on these systems can be extracted from neutron diffraction, with not many data to be gained from specific heat either. In the spin-glass phase magnetic moments are coupled by randomly distributed, both positive and negative, exchange interactions. Below the freezing temperature T_{f} the moments are blocked in a highly irreversible and metastable state characterized by the frustration of spins. At freezing temperature T_{f}, the χ' component exhibits a cusp-like anomaly, while χ'' shows a rapid onset followed by an inflection point and a weak maximum as the temperature is decreased. The main feature of the χ' anomaly is

its frequency dependence observed already below 1 kHz. This is in contrast to conventional or ferromagnetic materials, where the frequency dependence of susceptibility was found only in the MHz range. The empirical parameter X is used to express the T_f vs. f dependence, as following: $X = \Delta T_f/(T_f \Delta(\log f))$ [22]. The insulating spin-glasses show substantial T_f shift with frequency ($X \approx 0.01$) and χ'' equal to several % of χ'. For metallic spin-glasses, the frequency dependence is weaker and the related χ'' is less than 1% of χ'.

Having determined from the Argand plots the α parameter of distribution of relaxation times and the average relaxation time τ_c, one can evaluate the distribution of relaxation times as a function of $\log\tau$ for the investigated spin-glass. It appears that the half-width of such distribution remarkably increases upon cooling through T_f. Wide distribution of relaxation times is characteristic for the spin-glass phase. The other feature is a dramatic slow-down of the average relaxation time τ_c: for the two-dimensional spin-glass $Rb_2Cu_{1-x}Co_xF_4$ it was found that τ_c changes from 10^6 s at $T = 3$ K down to 10^{-10} s at $T = 7$ K [4].

3.5. Relaxation in superparamagnetic nanoparticles

At high temperatures, a system of magnetic single domain particles behaves like a paramagnet (superparamagnet) carrying a huge magnetic moment of the order of 10^3 μ_B. Magnetic moments fluctuate between up and down directions and change of the direction is a thermally activated process, with the relaxation time equal to

$$\tau = \tau_0 \exp(KV/k_BT), \tag{16}$$

where $\tau_0 = 10^{-9}$–10^{-11} s and ΔE equal to the product of the anisotropy constant and volume of the particle, $\Delta E = KV$.

Relaxation time τ of nanoparticles substantially increases upon cooling the sample. Assuming the period $\tau = 100$ s as the upper limit of observation of the magnetization change, one gets $KV/k_BT = 25$. The temperature, at which relaxation time of a given collection of nanoparticles equals 100 s is called the blocking temperature T_B and is determined as $T_B = KV/25k_B$. At $T < T_B$ magnetization processes are irreversible, characterized with thermoremanence, coercivity and long relaxation times. Mutual interactions between the particles as well as external pressure may increase the blocking temperature [23, 24] or lead to the collective behaviour of the spin-glass or ferromagnetic type [25].

An ideal system of magnetic nanoparticles showing superparamagnetic properties is ferritin. It is the iron storage protein, each particle is of *ca.* 12 nm diameter and consists of a core of antiferromagnetic ferrihydrite surrounded by a protein shell. The core is of about 7 nm in diameter and can contain up to 4500 Fe^{3+} ions, while a net magnetic moment of ≈ 300 μ_B comes from uncompensated iron spins, largely at the surface of the core [26].

Figure 11 shows the temperature dependence of χ' and χ'', measured with the different frequency of the oscillating field. Above 30 K χ' follows the Curie–Weiss law and $\chi'' = 0$. Below 30 K, the blocking of progressively smaller magnetic moments leads to decrease of χ' and to the onset of χ''. The maxima of the curves which occur at specific T_B shift to lower temperatures as frequency decreases. The activation energy determined from the Arrhenius formula (see inset) is $\Delta E = E_a/k_B = (415 \pm 15)$ K and $\tau_0 = 10^{-12}$ s. The shape of the hysteresis loop (not shown) is typical for an aggregate of particles influenced by the field coming from the surrounding particles.

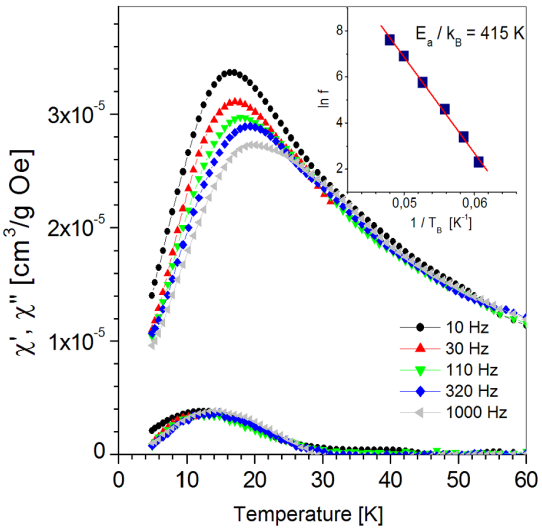

Fig. 11. Frequency dependent AC susceptibility of the horse spleen ferritin. Inset: determination of the activation energy from the $\ln f$ vs. $1/T$ Arrhenius plot.

4. Slow relaxation in low-dimensional molecular magnets

4.1. Research on single molecule magnets

A milestone in the field of molecular magnetism was the discovery of slow relaxation in the organometallic clusters, in which spins of metal ions are coupled giving a high-spin ground state. The most prominent example is the $[Mn_{12}O_{12}(O_2CCH_3)_{16}(H_2O)_4]4H_2O{\cdot}2CH_3COOH$ complex (Mn12) with the ground state spin $S = 10$. The characteristic feature of the cluster is a strong uniaxial anisotropy, expressed by the zero-field splitting parameter D. Anisotropy, combined with the high spin multiplicity gives rise to a large energy barrier between the up- and down-spin states. The work [27], which reported the dramatic increase of the relaxation time at low temperatures, according to the Arrhenius law with ΔE equal to $-DS^2$, entered upon the era of molecular nanomagnets. Due to the high barrier (ΔE for Mn12 is 65 K) and thus the long relaxation times, reaching months and years at temperature below $T \approx 2$ K, such anisotropic high-spin molecules were called single molecule magnets (SMM). They are of interest because of possible applications as magnetic memory or quantum computer units.

AC susceptibility of SMMs depends strongly on frequency. The temperature behaviour of χ' and χ'' for SMMs is like that for superparamagnets. Upon cooling the sample, χ_{AC} increases according to the Curie law, but at a certain, frequency dependent temperature, shows a drop at the blocking temperature $T_B \approx 3$ K. χ'' is indicative of slow relaxation of the magnetization, unable to keep in phase with the oscillating field [28]. The relaxation times determined from $\chi''(\omega)$ follow the Arrhenius exponential law with $\tau_0 = 2 \times 10^{-6}$ s, that is three orders of magnitude larger than that usually found in superparamagnets [29].

The analogy between superparamagnetic particles and SMMs is not full because the latter are quantum objects and show coherent effect of the quantum tunnelling of molecular spins over the barrier. The tunnelling of molecular spins is visible in a "staircase" hysteresis loop and in the DC-field-dependent AC susceptibility [29, 30]. The χ' and χ'' maxima observed at $H_n = nH_1$ with $n = 0$, 1, 2, where $H_1 = 4.1$ kOe, gave evidence of the field--tuned tunnelling between the excited magnetic states which are thermally populated [29, 30]. For another SMM, the Fe_8 cluster ($S = 10$), χ' also showed three distinct maxima regularly spaced in the magnetic field [30]. The maxima occurred for the same fields, for which a strong decrease of the spin–lattice relaxation time was estimated from the frequency-dependent AC susceptibility measurements. Because of quantum effects, the relaxation time τ does not grow exponentially to infinity but at low temperatures starts to saturate [29, 31].

4.2. Investigation of Mn-porphyrin based single chain magnet

Like in case of single molecule magnets, isolated one--dimensional (1D) magnetic molecular chains may also show the unique feature of slow magnetic relaxation and magnetic hysteresis without long range order [32–34]. By analogy to SMMs, this new class of nanomagnets is called single chain magnets (SCM)s. The first obtained SCM was the chiral $[Co(hfac)_2NITPhOMe)]$ ([Co(hfac)]) chain with the Ising anisotropy [32]. The search for SCMs was motivated with the increase of the blocking temperature, as magnetic coupling along the chain should impede the spin reversal and increase the activation energy. A large uniaxial anisotropy and strong magnetic coupling of spins along the chain promotes long relaxation times and such molecular chains can be individually magnetized. While ΔE for Mn12 SMM was 65 K, that for the [Co(hfac)] SCM is 152 K [32].

Compounds of the [MnTPP][TCNE] family of molecular chains based on Mn-porphyrin and TCNE-radical show a variety of relaxation behaviour. Magnetic properties of the substance may be tuned using various chemical modifications, e.g. substituting various functional groups R to the phenyl rings at the periphery of the porphyrin disc [35–37]. Mn(III) ion is located in the centre of the porphyrin complex and manganese spins ($S = 2$) and radical spins ($s = 1/2$) are strongly antiferromagnetically coupled along the chain, but, as there are no chemical bonds between the chains, the chains are magnetically (almost) isolated. Weak coupling between the chains which may be present is the dipolar coupling of the correlated chain segments. Ratio of the interchain- to intrachain interaction is $\approx 10^{-4}$ [38]. Magnetic properties of these low-dimensional systems may be tuned using various chemical modifications. The $[MnF_4TPP][TCNE]$ compound with fluorine substituted to porphyrin in the *ortho* position is a single-chain magnet (SCM) with blocking temperature $T_B = 6.6$ K [39].

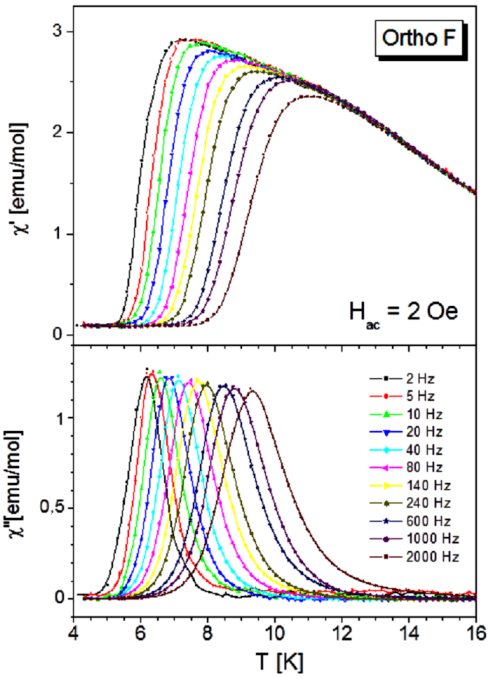

Fig. 12. Frequency dependent AC susceptibility of the $[MnF_4TPP][TCNE]$ single chain magnet; fluorine is substituted to porphyrin in the *ortho* position.

χ_{AC} of this compound shows strong dependence on frequency in accord with slow time decay of thermoremanence [39]. As may be seen from Fig. 12, upon decreasing temperature, χ' reaches the frequency dependent maximum and, when the moments cannot follow the oscillating field, abruptly falls down to zero (blocking). At the same time χ'' moves as a whole to lower temperatures. Value of the relative variation of the temperature T_p of the χ'' peak per decade of frequency, $X = (\Delta T_p/T_p)/\Delta(\log_{10} f)$, is equal to 0.128. This is much bigger than that of spin glasses and confirms the blocking phenomenon. Second and third harmonics of χ_{AC} are zero in the whole temperature range under study, which means that there is no spontaneous magnetic moment in the sample and that no phase transition occurs [40]. The χ'' vs. χ' Argand plots for $T = 6$ K up to $T = 9$ K are given in Fig. 13. They differ insignificantly from perfect semicircles and form arcs of size $(1 - \alpha)\pi$. The average distribution of relaxation times α is equal to 0.12, which means that in good approximation the

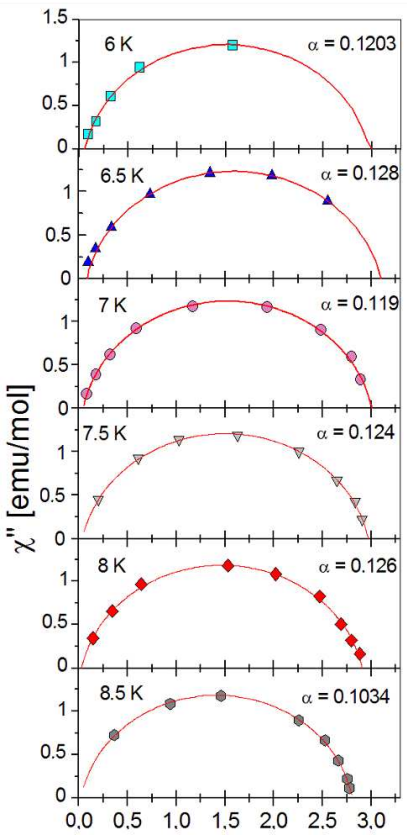

Fig. 13. Argand plots at several temperatures for the $[MnF_4TPP][TCNE]$ SCM obtained from the data shown in Fig. 12.

compound has a single relaxation time. This result is a fingerprint of the SCM behaviour [39].

As the lowest frequency of the AC field in the measurement shown in Fig. 12 was 2 Hz, the longest relaxation time registered was $\tau = 0.5$ s. In order to reach longer τ and to examine relaxation at $T < 5$ K, the dependence of M_{TRM} thermoremanence on time was measured. The stretched exponential Kohlrausch law

$$M_{\mathrm{TRM}}(t) = +M_0 \exp(-(t/\tau)^{1-n}), \quad 0 \le n \le 1 \tag{17}$$

was used to fit the data and extract τ vs. T. Having determined relaxation times in broad temperature range, one can calculate activation energy ΔE from the Arrhenius law. Figure 14 presents the plot $\ln\tau = \frac{\Delta E}{k_{\mathrm{B}}T} + \ln\tau_0$ of data gained from χ_{AC} and M_{TRM} time measurements. Energy barrier $\Delta E = E_{\mathrm{a}} = 117(5)$ K and $\tau_0 = 1.4 \times 10^{-10}$ s were obtained [39].

4.3. Slow relaxation and blocking in quasi 1D molecular magnets showing phase transition

As discussed in previous section, slow relaxation and blocking appeared in pure 1D molecular chain, where dipolar magnetic coupling between the chains was negligible. Low ratio of interchain- to intrachain interaction is crucial for the single chain magnet behaviour. In

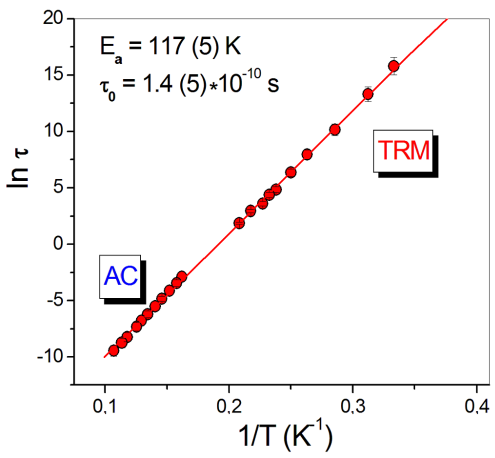

Fig. 14. Determination of the activation energy for $[MnF_4TPP][TCNE]$ SCM from the $\ln f$ vs. $1/T$ Arrhenius plot; results of χ_{AC} and M_{TRM} time measurements were used.

quasi-1D magnets, characterized with slightly larger ratio of interchain- to intrachain interactions, the slow relaxation and blocking will compete with a tendency to phase transition to the long range magnetic order. As a result, a complex phase situation would arise, which may be elucidated using the experimental possibilities of the AC susceptibility, i.e. wide spectrum of frequencies, measurements with zero- and nonzero applied DC field and testing the nonlinear susceptibilities.

Most members of the $[MnR_4TPP][TCNE]$ family of molecular chain compounds show anomalies in χ_{AC} at temperatures from the temperature range 10–30 K [36, 37]. When R is a long alcoxy group (OC_nH_{2n+1}, $n = 10$, 12, 14), the interchain spacing is very large (up to 30 Å) [41]. Despite the structural isolation of the chains the compounds show transition to the magnetically ordered state with $T_{\mathrm{c}} = 21.7$, 22.0, and 20.5 K, respectively [37]. Figure 15a presents the temperature dependence of χ_{AC} for $R = OC_{12}H_{25}$. A striking feature of this result is a strong dependence of susceptibility on the frequency ($X = 0.02$) and, simultaneously, a very sharp transition. When external DC field is applied, the AC peak reveals its double nature: the anomaly at T_{c} gradually disappears and the frequency dependent part is shifted to lower temperatures, where irreversibility of magnetization was also observed. As given in Fig. 15b, at $H = 5$ kOe the phase transition is completely destroyed and AC susceptibility shows only blocking, like that of the SCM-type with $\alpha_{\mathrm{av}} = 0.22$. From the Arrhenius plot one gets the activation energy $E_{\mathrm{a}} = 52$ K, with $\tau_0 = 3.5 \times 10^{-10}$ s (see Fig. 15b inset).

An example of the very strong influence of DC field on the relaxation is represented by the compound with $R = OCH_3$ ($T_{\mathrm{c}} = 8.7$ K), in which application of only 300 Oe makes the system to relax with the single relaxation time in the limits of the negligible distribution $\alpha = 0.08$ (see Fig. 16) [16]. All results shown

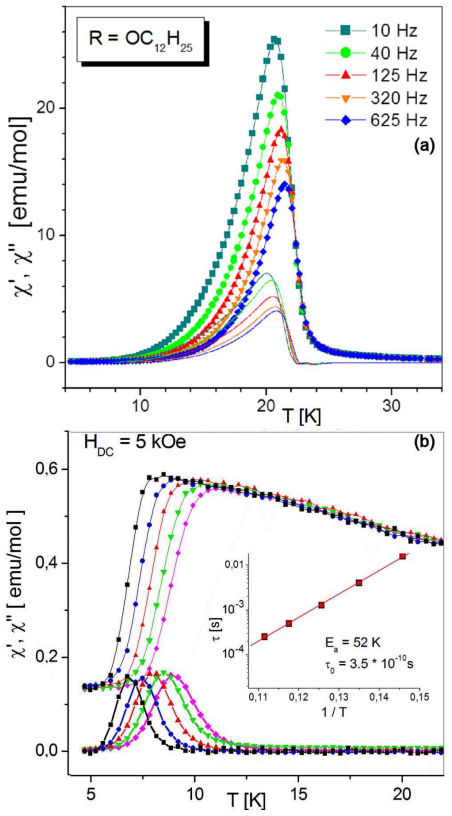

Fig. 15. (a) Frequency dependent AC susceptibility at $H_{DC} = 0$ for [MnR$_4$TPP][TCNE], where R = $OC_{12}H_{25}$ substituted into *Para* position [37]. (b) Effect of applied DC field of 5 kOe on the χ_{AC} of [MnR$_4$TPP][TCNE] where R = $OC_{12}H_{25}$ substituted into *para* position (see part (a)). Inset: $\ln f$ vs. $1/T$ plot [38].

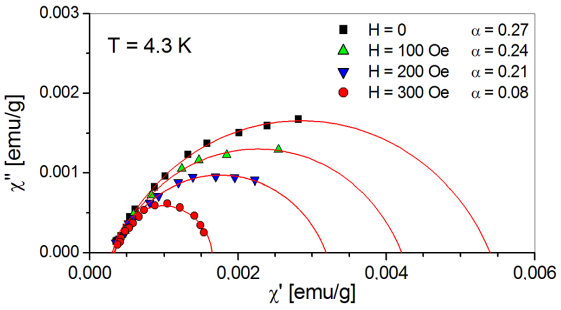

Fig. 16. Argand plots at several DC fields for [MnR$_4$TPP][TCNE], where R = OCH_3 substituted into *para* position [16].

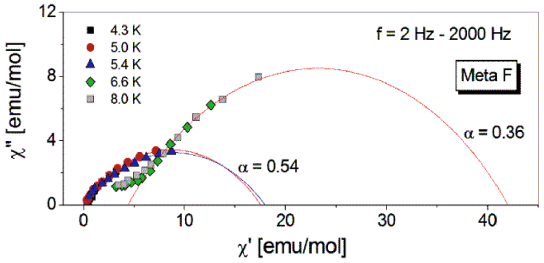

Fig. 17. Argand plot for [MnR$_4$TPP][TCNE], where R = F substituted into *meta* position; contribution from blocking and phase transition are visible [38].

above point to the fact that applied DC field attenuates the dipolar interchain coupling and brings in the magnetic isolation of the chains and thus the single chain magnet behaviour. The intermediate properties, showing both blocking (T_B = 5.4 K) and phase transition to the ordered phase (T_c = 8.8 K) is revealed by the [MnR$_4$TPP][TCNE] compound where fluorine is substituted to the *meta* position [38, 42]. Figure 17 shows the two contributions to the Argand plot: the left hand side arc with larger distribution of relaxation times corresponds to blocking, whereas the one with smaller α is due to phase transition. The different character of the χ_{AC} anomalies at T_B and at T_c was checked by the measurement of nonlinear susceptibilities. It was found that the second and third harmonic components were present only at T close to T_c, but were absent in the region of T_B. Therefore, blocking is not a phase transition in the thermodynamic sense. Parameter X for phase transition was 0.015, while the one for blocking was much larger and equaled 0.058 [38], similarly to that of cluster [22] or fractal spin-glasses [42].

On the basis of the presented results we conclude that slow relaxation is an inherent feature for all compounds of the [MnR$_4$TPP][TCNE] family. For the magnetically ordered compounds it is apparent in the AC susceptibility as a frequency dependent bump at temperatures below T_c or may show up in the high enough magnetic field. The superimposed DC magnetic field destroys the antiferromagnetic coupling between the chains and brings in magnetic isolation of the chains. A strong dependence of the AC susceptibility on frequency, observed in a number of ordered quasi-one-dimensional compounds, previously interpreted in the frames of spin (spin-cluster) glass [43], originates from SCM features. However, the true single chain magnet behaviour is a unique property, which rules out any magnetic transition to the collective phase.

Frequency dependent AC susceptibility measured at different applied DC fields may deliver still more information on magnetic relaxation. Field dependence of activation energy E_a and of the Arrhenius prefactor τ_0, determined from such measurements, should reflect the type of the mechanism of relaxation. Figures 18 and 19 present the effect of external magnetic field on E_a and on τ_0 for the single chain magnet [MnR$_4$TPP][TCNE], where R = *ortho*-F [39] and for the related compound with R = *meta*-F [38], which shows both blocking and phase transition to the ordered phase (see text above and Fig. 17). Despite the similar value of E_a at zero field, the dependence of activation energy on applied field looks quite different. As seen, for R = *ortho*-F, E_a at $H_{DC} \leq 1.5$ kOe does not change and for higher field gradually decreases.

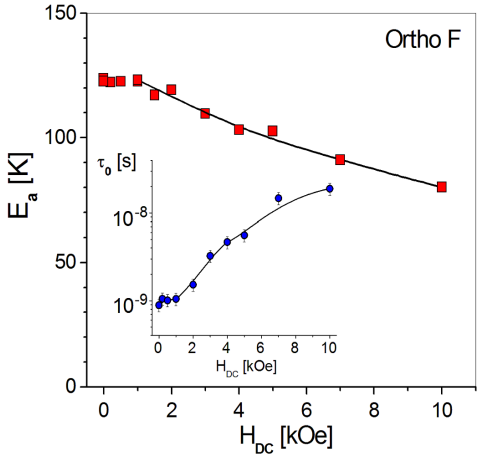

Fig. 18. Effect of applied magnetic field on activation energy for molecular single chain magnet [MnR_4 TPP][TCNE], where R = *ortho*-F. Inset: field dependence of time τ_0 [39]. Solid lines are guides.

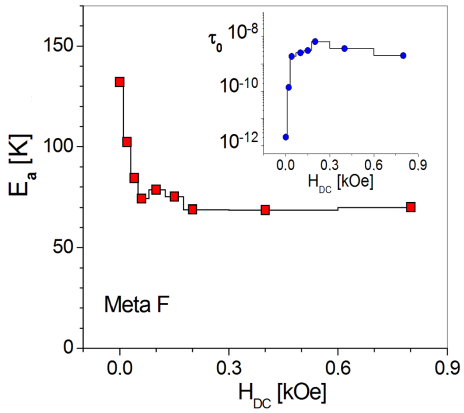

Fig. 19. Effect of applied magnetic field on activation energy for [MnR_4TPP][TCNE], where R = *meta*-F. Inset: field dependence of time τ_0 [38]. Solid lines are guides.

For R = *meta*-F, already at $H \approx 200$ Oe E_a drops down to the half value and then stays constant at the value $E_a = 70$ K, while the preexponential factor increases up to $\tau_0 \approx 5 \times 10^{-9}$ s and then does not change. This effect suggests that applied magnetic field divides magnetic chains into shorter segments and relaxation of terminal spins is observed [44].

5. Summary

The paper presents the short review of AC magnetic susceptibility results obtained for the representative conventional, molecular and low-dimensional magnets. It is shown that experimental possibilities of the AC technique, namely the varied frequency and amplitude of the oscillating field, applied DC field and detection of the nonlinear susceptibilities, allow to study in detail magnetic phase transitions and relaxation of the spin systems. Information may be obtained on: temperature of the long-range ordering, γ critical exponent, type of the magnetic transition, phase diagram in the DC field, relaxation time and/or its average value and distribution, activation energy and its dependence on the DC field; ferro-(ferri) and antiferromagnetic behaviour may be distinguished as well. The following examples were given:

- unique phase transition showing signatures of the Kosterlitz–Thouless transition in the quasi-2D $(tetrenH_5)_{0.8}Cu_4[W(CN)_8]_4{\cdot}xH_2O$ compound with XY anisotropy,
- antiferromagnetic commensurate to the sine-wave modulated incommensurate phase transition in the intermetallic compound $TbCo_2Si_2$ registered as an anomaly in the $d\chi'/dT$ dependence;
- spin glass transition above the Néel temperature of a frustrated antiferromagnet TbAuIn identified with higher harmonics of χ_{AC};
- dependence of χ_{AC} on the amplitude of the oscillating field tested with an aim to distinguish ferro-(ferri) and antiferromagnetic phases in rare earth metals and intermetallics (Th, GdPdIn, DyPdIn) and to determine the spin reorientation temperature (Gd);
- relaxation in the paramagnetic $CrK(SO_4)_2{\cdot}12H_2O$ alum placed in the DC magnetic field;
- relaxation and blocking in the ferritin superparamagnetic nanoparticles;
- slow relaxation in molecular nanomagnets: single molecule magnets and Mn-porphyrin based single chain magnet, distribution of relaxation times;
- slow relaxation and blocking in the [MnTPP][TCNE] family of molecular magnets showing phase transition;
- effect of applied magnetic field on activation energy in the single chain magnet and in the related quasi 1D molecular compound.

Results of the investigations have been complemented with a brief description of magnetic relaxation.

References

[1] W.J. De Haas, F.K. Du Pré, *Physica* **5**, 501 (1938); H.B.G. Casimir, F.K. du Pré, *Physica* **5**, 507 (1938).

[2] C.J. Gorter, L.C. Van der Marel, B. Bolger, *Physica* **21**, 103 (1955).

[3] H.A. Groenendijk, A.J. van Duyneveldt, *Physica* **115B**, 41 (1982);A.J. van Duyneveldt, *J. Appl. Phys.* **53**, 8006 (1982).

[4] C.A.M. Mulder, A.J. van Duyneveldt, J.A. Mydosh, *Phys. Rev. B* **23**, 1384 (1981); C. Dekker, A.F.M. Arts, H.W. de Wijn, A.J. van Duyneveldt, J.A. Mydosh, *Phys. Rev. B* **40**, 11243 (1989).

[5] T. Ishida, R.B. Goldfarb, *Phys. Rev. B* **41**, 8937 (1990); F. Gömöry, *Supercond. Sci. Technol.* **10**, 523 (1997).

[6] D. Pinkowicz, R. Podgajny, R. Pełka, W. Nitek, M. Bałanda, M. Makarewicz, M. Czapla, J. Żukrowski, Cz. Kapusta, D. Zając, B. Sieklucka, *Dalton Trans. Issue*, 7771 (2009).

[7] M. Bałanda, R. Pełka, T. Wasiutyński, M. Rams, Y. Nakazawa, T. Korzeniak, M. Sorai, *Phys. Rev. B* **78**, 174409 (2008).

[8] M. Bałanda, T. Korzeniak, R. Pełka, R. Podgajny, M. Rams, B. Sieklucka, T. Wasiutyński, *Solid State Sci.* **7**, 1113 (2005).

[9] N.D. Mermin, H. Wagner, *Phys. Rev. Lett.* **22**, 1133 (1966).

[10] J.M. Kosterlitz, D.J. Thouless, *J. Phys. C* **6**, 1181 (1973).

[11] A. Szytuła, M. Bałanda, B. Penc, M. Hofmann, *J. Phys., Condens. Matter* **12**, 7455 (2000).

[12] Ł. Gondek, A. Szytuła, M. Bałanda, W. Warkocki, A. Serczyk, M. Gutowska, *Solid State Commun.* **136**, 26 (2005).

[13] A. Szytuła, W. Bażela, Ł. Gondek, T. Jaworska-Gołąb, B. Penc, N. Stüsser, A. Zygmunt, *J. Alloys Comp.* **336**, 11 (2002).

[14] M. Bałanda, A. Szytuła, M. Guillot, *J. Magn. Magn. Mater.* **247**, 345 (2002).

[15] W.C. Koehler, *J. Appl. Phys.* **36**, 1078 (1965).

[16] M. Bałanda, in: *Relaxation Phenomena. Liquid Crystals, Magnetic Systems, Polymers, High-T_c Superconductors, Metallic Glasses*, Eds. W. Haase, S. Wróbel, Springer, 2003, p. 96.

[17] J.M.D. Coey, V. Skumryev, K. Gallagher, *Nature* **401**, 35 (1999).

[18] H.B.G. Casimir, F.K. du Pré, *Physica* **5**, 507 (1938); R. Kubo, T. Nagamiya, *Solid State Physics*, McGraw-Hill, New York 1969.

[19] A.H. Morrish, *The Physical Principles of Magnetism*, Wiley, New York 1965.

[20] H.A. Groenendijk, A.J. van Duyneveldt, R.D. Willet, *Physica B* **101**, 320 (1980).

[21] D.-X. Chen, V. Skumryev, J.M.D. Coey, *Phys. Rev. B* **53**, 15014 (1996).

[22] J.A. Mydosh, *Spin Glasses: n Experimental Introduction*, Taylor&Francis, London 1993.

[23] J. Dai, J.-Q. Wang, C. Sangregorio, J. Fang, E. Carpenter, J. Tang, *J. Appl. Phys.* **87**, 7397 (2000).

[24] K. Nadeem, H. Krenn, T. Traussnig, R. Würschum, D.V. Szabó, I. Letafsky-Papst, *J. Magn. Magn. Mater.* **323**, 1998 (2011).

[25] J.L. Dormann, D. Fiorani, R. Cherkaoui, E. Tronc, F. Lucari, F. D'Orazio, L. Spinu, M. Nogues, H. Kachkachi, J.P. Jolivet, *J. Magn. Magn. Mater.* **203**, 23 (1999).

[26] F. Luis, E. del Barco, J.M. Hernández, E. Remiro, J. Bartolomé, J. Tejada, *Phys. Rev. B* **59**, 11837 (1999).

[27] R. Sessoli, D. Gatteschi, A. Caneschi, M.A. Novak, *Nature* **365**, 141 (1993).

[28] F.L. Mettes, F. Luis, L.J. de Jongh, *Phys. Rev. B* **64**, 174411 (2001).

[29] L. Thomas, F. Lionti, R. Ballou, D. Gatteschi, R. Sessoli, B. Barbara, *Nature* **383**, 145 (1996).

[30] F. Luis, J. Bartolome, J.F. Fernandez, J. Tejada, J.M. Hernandez, X.X. Zhang, R. Ziolo, *Phys. Rev. B* **55**, 11448 (1997).

[31] A. Caneschi, D. Gatteschi, C. Sangregorio, R. Sessoli, L. Sorace, A. Cornia, M.A. Novak, C. Paulsen, W. Wernsdorfer, *J. Magn. Magn. Mater.* **200**, 182 (1999).

[32] A. Caneschi, D. Gatteschi, N. Lalioti, C. Sangregorio, R. Sessoli, G. Venturi, A. Vindigni, A. Rettori, M.G. Pini, M.A. Novak, *Europhys. Lett.* **58**, 771 (2002).

[33] R. Clérac, H. Miyasaka, M. Yamashita, C. Coulon, *J. Am. Chem. Soc.* **124**, 12837 (2002).

[34] H. Miyasaka, R. Clerac, K. Mizushima, K.-I. Sugiura, M. Yamashita, W. Wernsdorfer, C. Coulon, *Inorg. Chem.* **42**, 8203 (2003).

[35] E.J. Brandon, D.K. Rittenberg, A.M. Arif, J.S. Miller, *Inorg. Chem.* **37**, 3376 (1998).

[36] M. Fardis, G. Diamantopoulos, G. Papavassiliou, K. Pokhodnya, J.S. Miller, D.K. Rittenberg, C. Christides, *Phys. Rev. B* **66**, 064422 (2002).

[37] M. Bałanda, K. Falk, K. Griesar, Z. Tomkowicz, W. Haase, *J. Magn. Magn. Mater.* **205**, 141 (1999).

[38] M. Bałanda, Z. Tomkowicz, W. Haase, M. Rams, *J. Phys., Conf. Ser.* **303**, 012036 (2011).

[39] M. Bałanda, M. Rams, S.K. Nayak, Z. Tomkowicz, W. Haase, K. Tomala, J.V. Yakhmi, *Phys. Rev. B* **74**, 224421 (2006).

[40] T. Bitoh, K. Ohba, M. Takamatsu, T. Shirane, S. Chikazawa, *J. Magn. Magn. Mater.* **154**, 59 (1996).

[41] K. Griesar, M.A. Athanassopoulou, E.A. Soto Bustamante, Z. Tomkowicz, A. Zaleski, W. Haase, *Adv. Mater.* **9**, 45 (1997).

[42] Z. Tomkowicz, M. Rams, M. Bałanda, N. Nojiri, V. Kataev, S.K. Nayak, J.V. Yakhmi, W. Haase, *Inorg. Chem.* **51**, 9993 (2012).

[43] S.J. Etzkorn, W. Hibbs, J.S. Miller, A.J. Epstein, *Phys. Rev. Lett.* **89**, 207201 (2002).

[44] L. Bogani, A. Caneschi, M. Fedi, D. Gatteschi, M. Massi, M.A. Novak, M.G. Pini, A. Rettori, R. Sessoli, A. Vindigni, *Phys. Rev. Lett.* **92**, 207204 (2004).